Numerical Studies of Micro-Cathode Arc Thruster Plume Expansion

IEPC-2015-57/ISTS-2015-b-57

Presented at Joint Conference of 30th International Symposium on Space Technology and Science, 34th International Electric Propulsion Conference and 6th Nano-satellite Symposium
Hyogo-Kobe, Japan
July 4–10, 2015

Lubos Brieda*
Particle In Cell Consulting LLC, Falls Church, VA, 22046

Michael Keidar†
The George Washington University, Washington, D.C. 20052

In this paper we report on a numerical model of the plume formation and expansion of a micro-cathodic arc thruster (μCAT) developed at the George Washington University. This thruster is available in two designs, with one utilizing a magnetic field to trap and turn electrons generated at the cathode spot. The resulting electric field then works to turn and accelerate the Titanium ions, which generate the thrust. In this paper we present latest results from a fully-kinetic simulation of the thruster. The simulation resolves the full domain, but due to high densities in the cathode spot, we had to utilize artificial permittivity. Then perhaps due to this fix, ion dynamics does not seem to be properly resolved.

I. Introduction

For the past several years, the Micropropulsion and Nanotechnology Laboratory at the George Washington University has been developing a novel thruster for microsatellites based on the ablative vacuum arc technology. This micro-cathode arc thruster (μCAT) has been summarized in a number of papers, including 1–5. Currently, the thruster is being flight-qualified aboard the Naval Acadamy's BRICSat,[6] with additional flight time expected aboard the ARC PhoneSat.[7] The thruster has undergone several modifications, and is currently available in two designs: a ring-type and an axial variant. In this paper, we consider only the original ring-type concept, which is shown in Figure 1. The thruster consists of a tubular Titanium cathode, an insulator, and a copper anode. An inductor-driven power supply generates pulses which results in a vacuum arc breakdown, and ablation of the cathode material in the form of a dense Titanium plasma. A spring actuator pushes the eroded cathode forward, providing the thruster with a continuous supply of propellant. This design provides the mission designer with flexibility to size the thruster to specific mission propulsion requirements by simply adjusting the length of the cathode.

The disadvantage of the ring design is that in absence of an additional force, the cathodic plume expands primarily in the radial direction. To increase the propulsive force, the thruster is surrounded by an electromagnet that generates magnetic field with field lines primarily aligned with the thrust axis. The strength of the field is selected such that only the electrons are magnetized. The resulting ambipolar field then provides the force to turn the ions into the axial direction, thus generating thrust. The electromagnet furthermore provides the mission operator with capability to adjust thrust and Isp by varying the coil current. This capability is not found in traditional vacuum arc thrusters. Additionally, the magnetic field aids in uniform ablation of the cathode.

The miniature size and power requirements of this device make it suitable for a range of nanosatellites that traditionally would not be suitable candidates for on-board propulsion. However, as the demand for

*Contact email: lubos.brieda@particleincell.com
†Professor, Mechanical and Aerospace Engineering

this and other similar thrusters grows, it is necessary to obtain a better understanding of its behavior, plume properties, and any possible contamination concerns. The small size makes it difficult to utilize traditional tools, such as Faraday or Langmuir probes. The existing experimental effort typically consisted of utilizing a large segmented collector plate to measure current and rotation velocity as a function of segment location. Additional measurements were made by weighing the thruster to estimate the mass flow per pulse, and by utilizing a thrust scale to measure thrust. However, a detailed study of the plume profile, especially at significant distance from the device remains a challenge. Some representative measurements have been summarized in Figure 2.

In parallel with the experimental effort, Particle In Cell Consulting LLC (PIC-C) has been developing a generalized two-dimensional plasma and rarefied gas simulation code, Starfish.[8] The μCAT is a good candidate for numerical analysis due to its small size and interesting physics. The numerical effort was first introduced in 9. This paper summarizes the numerical effort to date. The goal of this effort is to develop an end-to-end simulation, capturing the plasma discharge from the cathode spot to the near plume. As indicated in the following paragraphs, the existing modeling is concerned with the internal near-cathode discharge. We describe the numerical model and simulation inputs in the next section. We subsequently present the preliminary results. The paper is concluded with the future work.

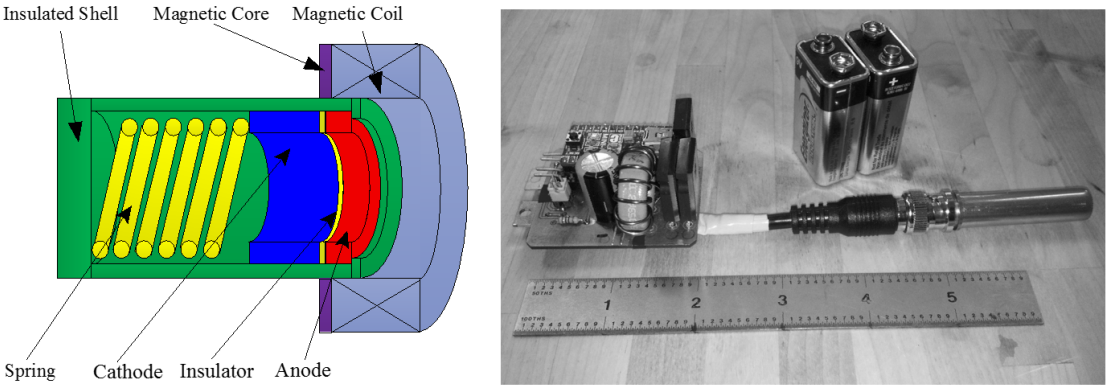

Figure 1. Schematic drawing and a photograph of the μCAT. Plasma is formed at the cathode/insulator interface and is turned axially by the magnetic field. Figure from 1.

II. Numerical Model

A. Simulation Code

The simulations presented in this paper were performed using the Starfish simulation code. Starfish is a 2D Cartesian / axisymmetric code for modeling a wide range of plasma and rarefied gas problems. The code consists of a core module providing common functionality, as well as basic algorithms for the particle-in-cell (PIC) and Monte Carlo collisions (MCC) methods. The capabilities of the core module can be expanded by plugins which are linked against the core library. The individual plugins provide features such as DSMC, CFD, MHD, surface chemistry, as well as advanced solvers for EP devices. The simulation settings are specified via several XML input files which provide the details of computational domain, surface definition, material types, injection models, and material interaction. The main simulation file also specifies the overall algorithm, and executes additional commands such as those needed to load magnetic field, specify solver parameters, and set the diagnostic output properties.

B. Magnetic Field Profile

Starfish supports multiple meshes and for this simulation we selected a collection of three rectilinear grids of varying refinement as shown in Figure 3. From right to left, the meshes describe the internal region dominated by the cathode spot formation and turning of the ion beam, the middle acceleration zone, and external near-field. In this paper we concentrate only on the internal region, with the full simulation still remaining as future work. This figure also shows the magnetic field profile. The magnetic field was obtained

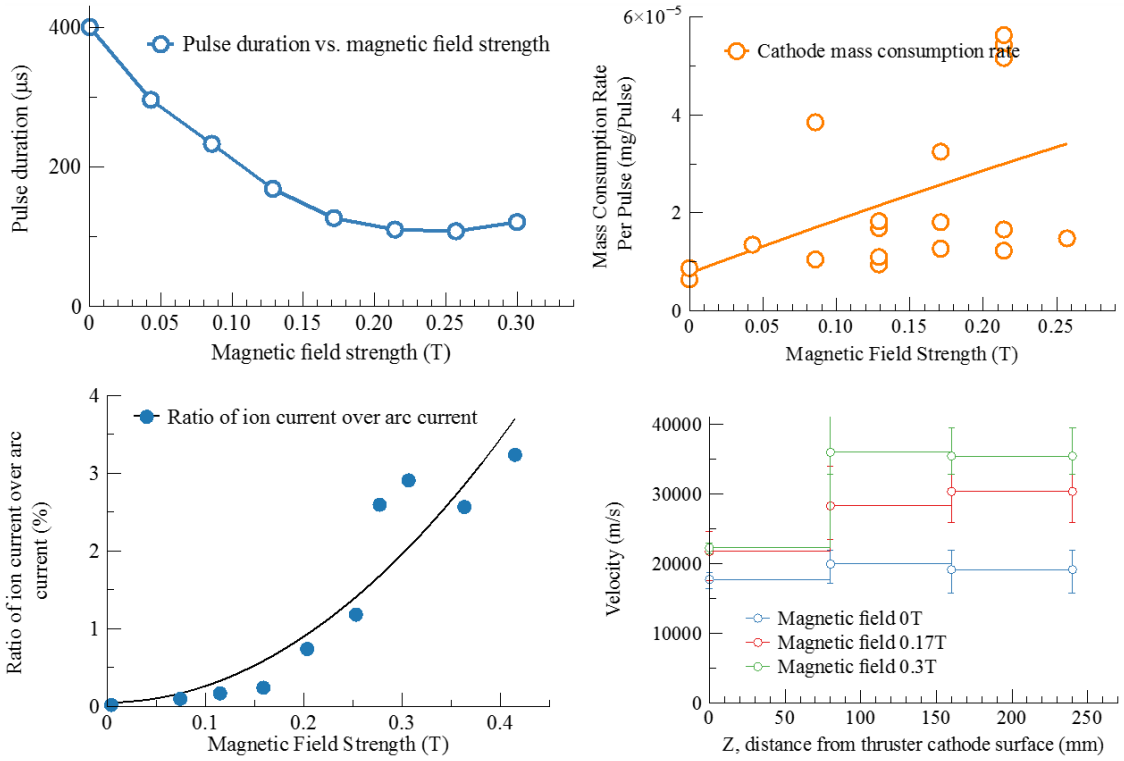

Figure 2. Summary of thruster operating parameters. Figure from 1.

using the FEMM simulation package. We considered three coil current settings: 5A, 10A, and 20A, resulting in approximate field strengths of 0.13, 0.27, and 0.54T in the acceleration zone.

C. Simulation Inputs

The simulation domain consisted of linear splines denoting the magnet, anode, insulator, cathode, and the cathode spot, as shown in Figure 3. Although the thruster is axisymmetric in nature, the method of operation is not axisymmetric in the time span of a single cathode spot. The cathode spot forms at an arbitrary location along the cathode insulator interface and rotates during the discharge cycle. As shown in Figure 2, the pulse duration varies from 400s to about 150μs based on the magnetic field strength. Since Starfish is a 2D code, it is not possible to resolve this spatial non-uniformity. Instead, we made the assumption that the injected material is distributed uniformly over the circumference of the thruster.

As noted in [10] cathode spots in arc discharges are expected to be in sub-millimeter range, with typical spot radius noted as 50 μm. The plasma density is on the order of 10^{26} m^{-3}, clearly beyond the application of kinetic methods. In our simulation, we took an additional liberty and set the spot diameter as 1mm. Since we further assumed axial symmetry, the expected effective density was reduced by almost 4 orders of magnitude. However, as the above formulation is based on a simple model, we decided to utilize experimental data to determine the injection properties.

We can obtain the thruster mass flow rate by considering the average mass lost during a single operational pulse. In [1], authors indicate that the mass decreased by 3.8×10^{-6}mg over a 120μs pulse. Hence, $\dot{m} = 3.8 \times 10^{-11}\text{kg}/120 \times 10^{-6}\text{s} = 3.166 \times 10^{-7}$kg/s. We next assume that this mass is expelled by the thruster in the form of doubly-ionized Titanium ions [11]. The corresponding current is thus $I = 2e(\dot{m}/m_{Ti}) = 1.27$A. Figure 4 shows the current profile as a function of time for a single pulse. This particular data shows a pulse of a longer duration, however, the general shape and magnitudes are similar for all considered magnetic fields. In our work, we limited ourselves to this 400s pulse and applied it to all cases, regardless of the specified magnetic field strength. The current profile in Figure 4 was digitized and fitted with an exponential trend line $I(t) = 60\exp(-0.013t)$, where t is in μs. The fit is shown in Figure 4 with a dashed line. The exponential

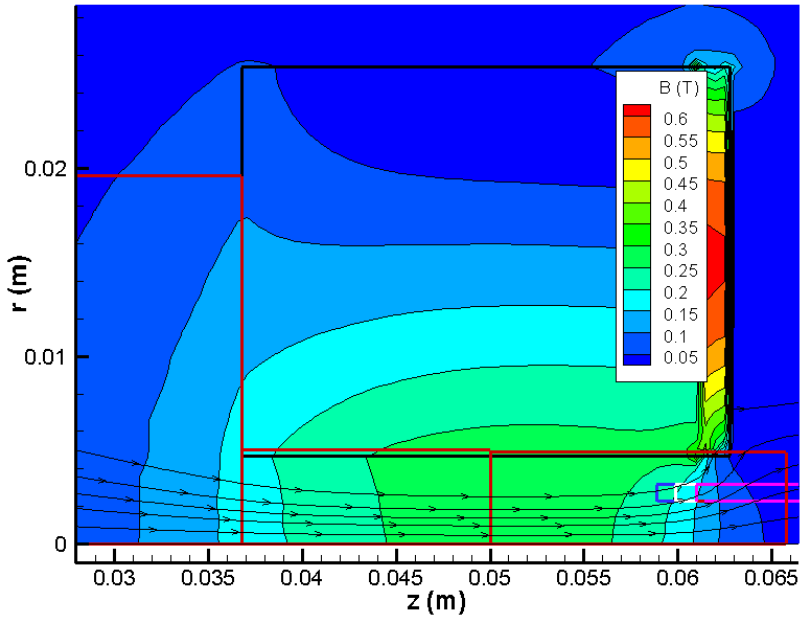

Figure 3. A conceptual simulation domain capturing the thruster and the near-plume region. Contours and streamlines show the magnetic field. The three meshes are shown in red. Anode, insulator, cathode, and magnet are shown in blue, white, purple, and black, respectively. The cathode spot may be seen at the insulator cathode interface.

profile allows us to easily compute the mean arc current as $\bar{i} = \left(\int_{t_1}^{t_2} I \mathrm{d}t\right) / (t_2 - t_1) = 11.47\mathrm{A}$.

Reference [1] also indicates that at 0.3T, the beam to arc current ratio was 3%. Hence, we would expect beam current of approximately 0.344A. This value is smaller than the predictions above obtained from mass loss consideration, indicating that a fraction of the expelled mass may be emitted in the form of a non-ionized propellant. In this work we do not consider neutral atoms, and hence we utilized the latter current to set the mass flow rates for ions and electrons. The corresponding values were 8.53×10^{-8} and 1.96×10^{-12} kg/s, respectively.

Starfish supports both kinetic and fluid materials. In this case we utilized the kinetic approach for both ions and electrons. The materials were injected into the simulation domain via a Maxwellian-like source attached to the cathode spot surface component. As indicated in [10], the ionization of the ablated material happens a short distance from surface, however, this detail was not modeled and instead we treated the spot as a source of both ions and electrons. The source mass flow rate was modulated according to the exponential current decay, $\dot{m} = m_0 I(t)/\bar{I}$.

D. Computational Domain

In this work, we considered the "full" domain, and also a reduced domain, as shown in Figure 5. The full domain consisted of three rectilinear meshes with an increasing cell size. This setup allowed us to capture a larger physical space while maintaining a reasonable number of unknowns. The potential is solved by a Gauss-Seidel solver which communicates boundary data between meshes in a fashion similar to parallel processing.

III. Results

A. Virtual Anode

Figure 6 indicates a major difficulty that was encountered in this kinetic modeling. This plot shows the plasma potential computed in the absence of a magnetic field and utilizing physical simulation parameters. Due to the large plasma density, the Debye length is approximately 10^{-5} m. Resolving the internal thruster region at this resolution would require over half a million cells, which is beyond the practical limit for the

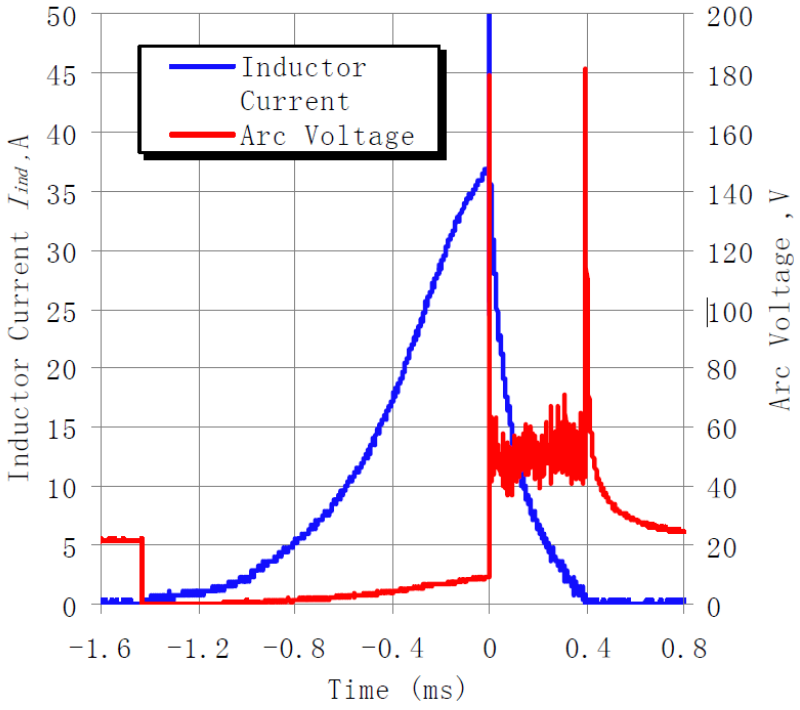

Figure 4. Typical current voltage profile. The red dashed line illustrates the exponential curve used to modulate the source mass flow rate.

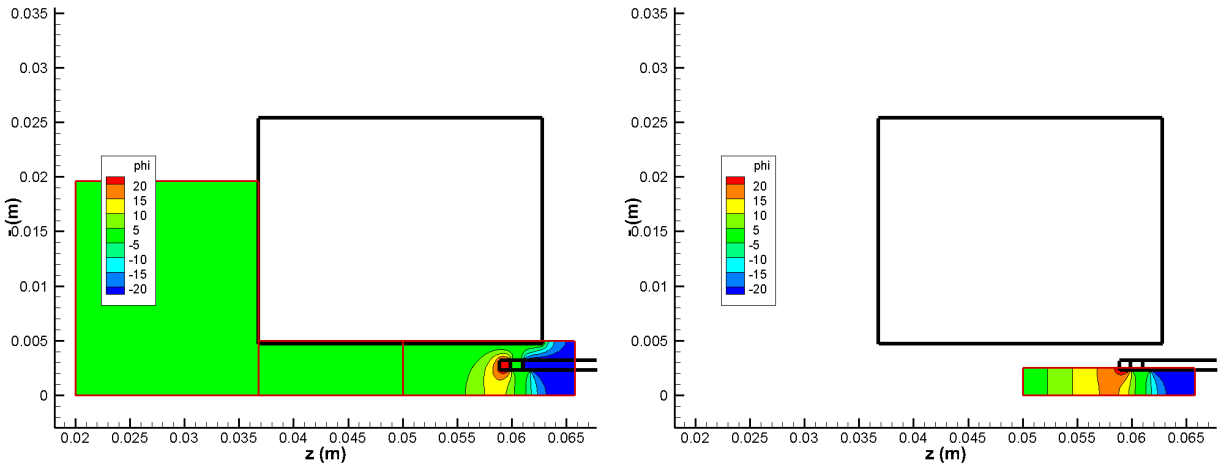

(a) Full domain

(b) Reduced domain

Figure 5. Initial potential on the two considered computational domains.

current Starfish version, which has not yet been fully parallelized. The computational time is driven by the Poisson solver convergence rate, and coupled with the large number of time steps that were required due to a small electron time step, the predicted wall time was deemed unacceptable. Unfortunately, in the absence of a sufficiently fine mesh, the simulation develops a virtual anode, which is a relatively common problem in fully-kinetic plasma simulations. The virtual anode develops due to local charge density exceeding the Child Langmuir limit. A finer mesh helps resolve the charge density variations since in the PIC method, no detail is available at the spatial resolution higher than the mesh size. As seen in Figure 6, the virtual anode demonstrates itself in the formation of a region with large positive plasma potential just outside the cathode spot. The resulting electric field retards the motion of ions, resulting in their backflow to the cathode. To mitigate this effect, we tried number of approaches, including utilizing a finer mesh, which was found to be impractical. Alternate approaches included a charge density limiter and an artificial increase to the permittivity of free space, ϵ_0. Permittivity appears in the Poisson equation,

$$\nabla^2\phi = -\frac{\rho}{\epsilon_0} \tag{1}$$

and hence the adjustment is analogous to an artificial reduction in plasma density $n = \rho/eZ$. This was the approach that was utilized in this work. We solved $\nabla^2\phi = -\rho/(\epsilon_r\epsilon_0)$, where $\epsilon_r = 10^4$.

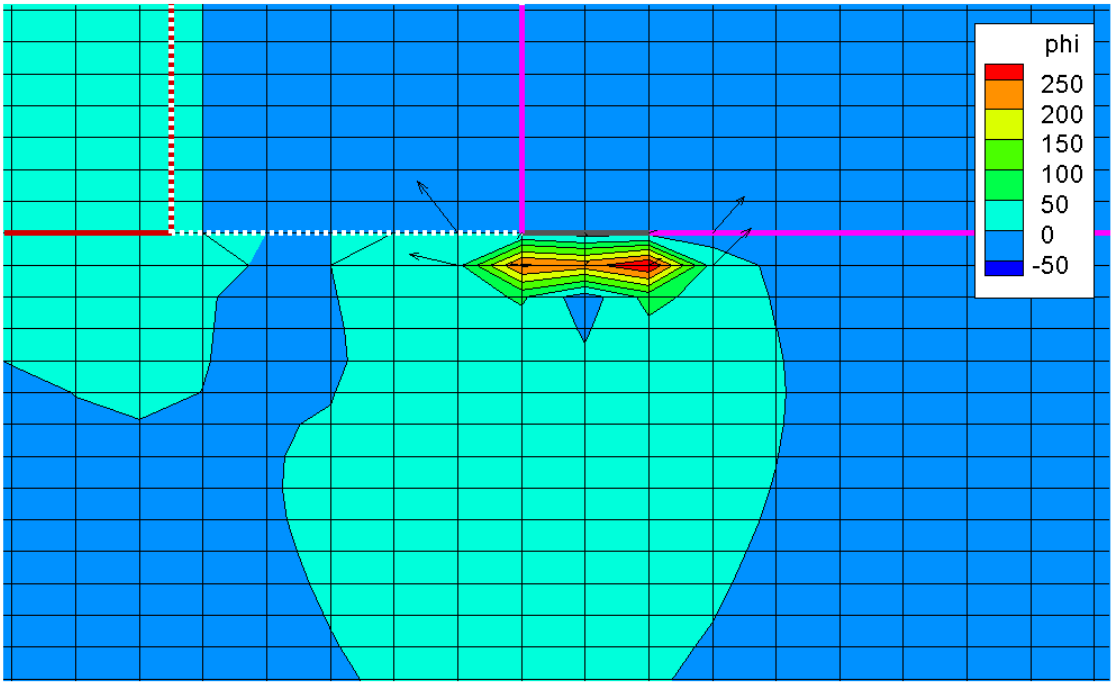

Figure 6. Formation of a virtual anode due to insufficient mesh resolution. Vectors indicate electric field.

B. Effect of Magnetic Field

The preliminary results are plotted in Figures 7 and 8. These figures compare the plasma potential, and ion and electron densities for the case with and without a magnetic field. Both sets of figures were plotted after approximately 70,000 time steps at $\Delta t = 2 \times 10^{-11}$s to indicate the corresponding behavior. As predicted, the magnetic field results in magnetization of electrons. Although not shown here, animation results clearly indicate the electrons drifting back and forth along the field line according to the evolution of the ion density. The confinement of the electrons to the field line results in a region of large negative charge. This then demonstrates itself as a narrow channel in the potential profile. It is believed that this channel is responsible for the transport of the ion beam from the thruster. We can in fact see the initial stages of the beam turning in Figure 6b). However, we also see a significant ion loss to the insulator. In this preliminary study, the insulator was modeled as a Dirichlet boundary set at 0V. The anode and cathode potentials were

-25V and +25V, respectively. A small potential hill that forms radially inward from the cathode spot is responsible for slowing down ions as they pass through the magnetic field containing the electrons. This hill is analogous to the virtual anode described previously. However, in this case, it is a physical structure arising from the charge separation due to magnetized electrons. It is believed that the reflected ions should next turn into the channel created by the electrons, and in fact, many do. However, a noticeable fraction of ions is instead collected by the insulator. As part of future work, we will investigate a more rigorous model for the insulator, including surface charging and surface emission.

Figure 8 plots obtained in the absence of a magnetic field. Immediately we can see that the electrons are no longer magnetized. Instead, their distribution is now governed by the local plasma potential arising from the presence of the anode, and from the presence of the ion beam. We also see axial diffusion of the ion beam near the thruster centerline. This diffusion is a byproduct of our axi-symmetric model and may not be present in the physical device. In the absence of repulsive forces, number density would grow continuously as we approach the centerline due to concentration of mass into a smaller volume and the uniform circumferential plasma generation. The plasma potential responds to this non-physical anomaly by an increase in the centerline potential. This repulsive force then reduces flux of ions. Animations indicate that in fact, in the absence of the magnetic field, the thruster operates at an oscillatory mode with high-frequency bursts of emitted ions. These bursts are followed by a period marked with decreasing centerline plasma potential and ion accumulations. It is not yet clear if this oscillatory behavior is a feature of a real thruster or an artifact of the axisymmetric model.

C. Full Domain

Preliminary results on the full domain are shown in Figure 9, 10, and 11. Although the simulations correctly resolve the magnetization of the electrons, the ion dynamics seem to be driven to a greater extend by plasma pressure than ambipolar diffusion. This could be an artifact of the used artificial permittivity. Ions seem to be diffusing from the thruster instead of being accelerated by the electric field.

IV. Conclusion

In this paper we updated on the progress of modeling a miniature ablative vacuum arc thruster suitable for a range of nanosatellite missions using a fully kinetic model. The objective of the simulation is to perform an end-to-end model from the cathode spot to the thruster near-plume. So far, we have been able to resolve the ion and electron dynamics in the near plume region. However, due to high densities in the cathode spot, we had to utilize artificial permittivity which may be affecting the solution.

Although a number of outstanding issues still remain, the simulation results to date are promising. The results indicate that the electric field due to the magnetized electrons is responsible for turning and ejecting the ablated titanium ions from the device. In the absence of a magnetic field, the device thrust is governed by diffusion. For future work, we plan to develop a mesh refinement capability to help capture details of the high density cathode region as well as parallelize the simulation code, allowing us to tackle larger simulation domains.

References

[1]Keidar, M., Zhuang, T., Shashurin, A., andDereck Chiu, G. T., Lukas, J., Haque, S., and Brieda, L., "Electric propulsion for small satellites," *Plasma Phys. Control. Fusion*, Vol. 57, No. 014005, 2015.

[2]Zhuang, T., Shashurin, A., and Keidar, M., "Performance measurements of Micro-Cathode Arc Thruster," *IEEE Trans. Plasma Science*, Vol. 39, No. 11, 2011.

[3]Zhuang, T., Shashurin, A., Keidar, M., and Belis, I., "Circular periodic motion of plasma produced by a small-scale vacuum arc," *Plasma Sources Science and Technology*, Vol. 20, No. 015009, 2011.

[4]Zhuang, T., Shashurin, A., Beilis, I., and Keidar, M., "Ion velocities in a micro-cathode arc thruster," Vol. [19.

[5]Zhuang, T., Shashurin, A., Haque, S., and Keidar, M., "Performance characterization of the micro-Cathode Arc Thruster and propulsion system for space applications," *46th AIAA Joint Propulsion Conference*, Cleveland, OH, 2010.

[6]Lukas, J., Teel, G., Haque, S., Shashurin, A., and Keidar, M., "Thruster Subsystem Design for the Ballistic Reinforced Communication Satellite (BRICSat-P)," 2014.

[7]Haque, S. E., Teel, G., Tintore, O., Trinh, G. T., Uribe, E., Perez, A. D., Agasid, E. F., and Keidar, M., "Applications of Micro-Cathode Arc Thruster as in-space propulsion subsystem for PhoneSat," *Aerospace Conference, 2014 IEEE*, IEEE, 2014, pp. 1–18.

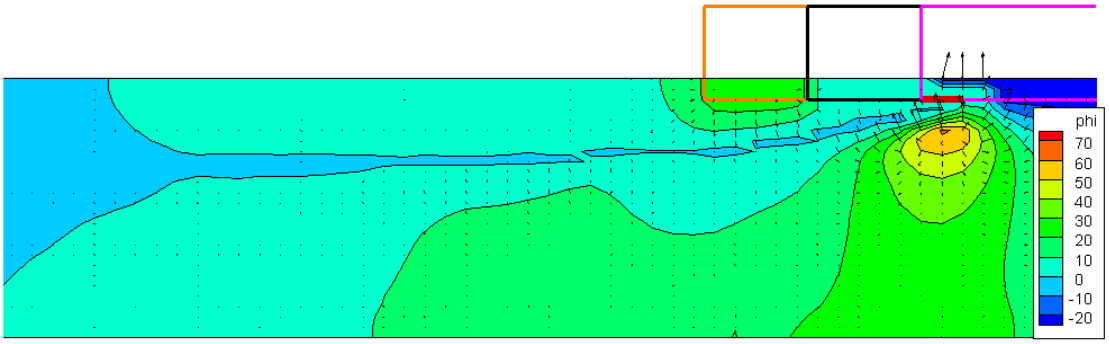

(a) Plasma Potential

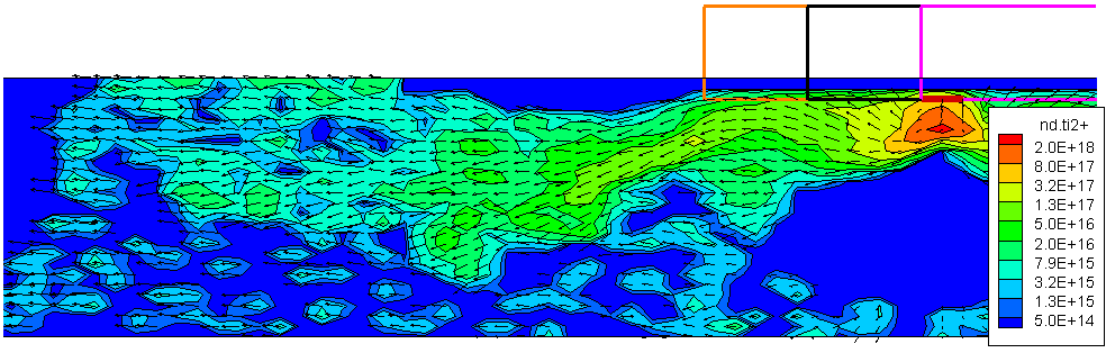

(b) Ion Density

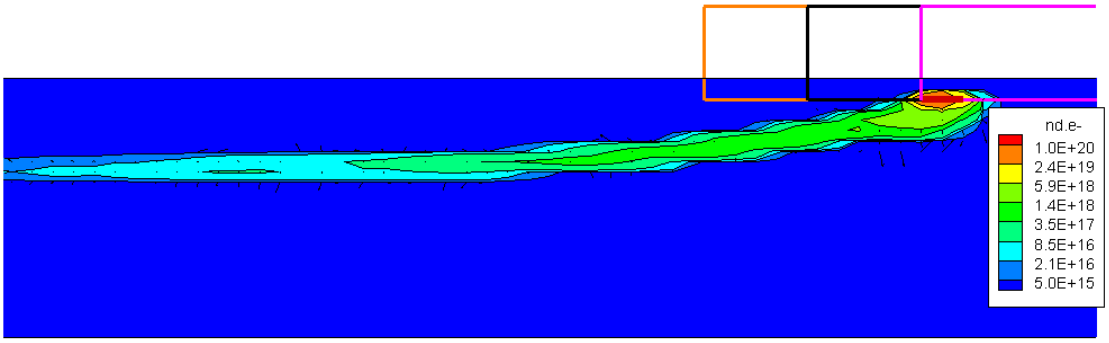

(c) Electron Density

Figure 7. Preliminary results showing plasma potential, ion density, and electron density with magnetic field 0.3T

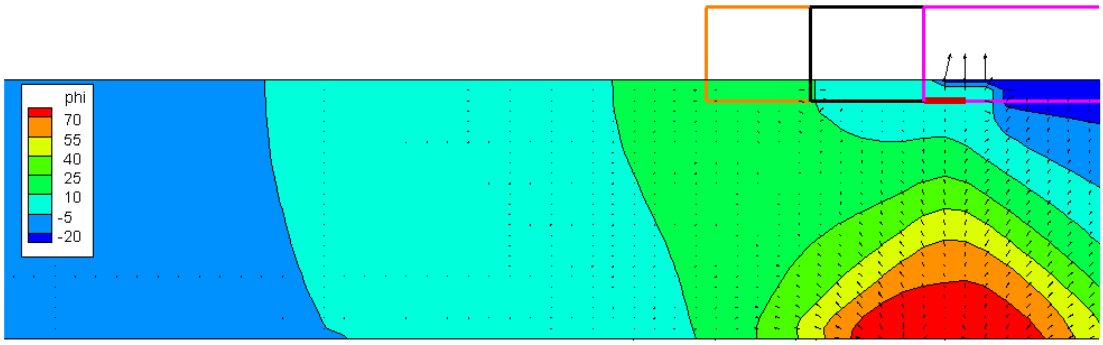

(a) Plasma Potential

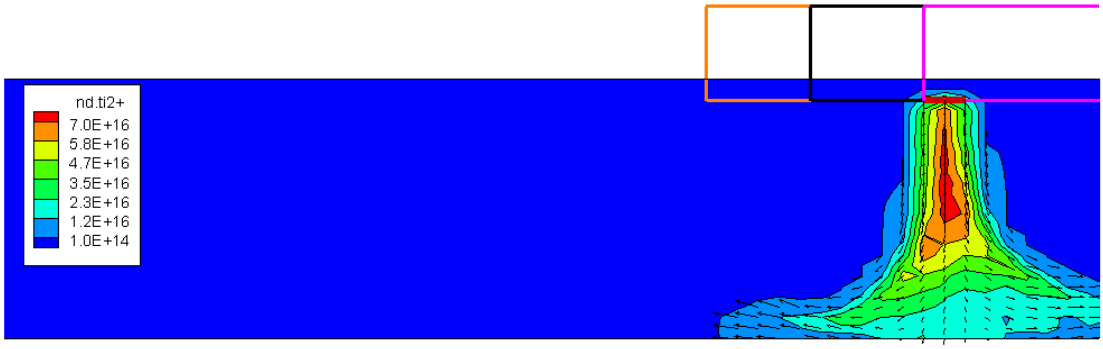

(b) Ion Density

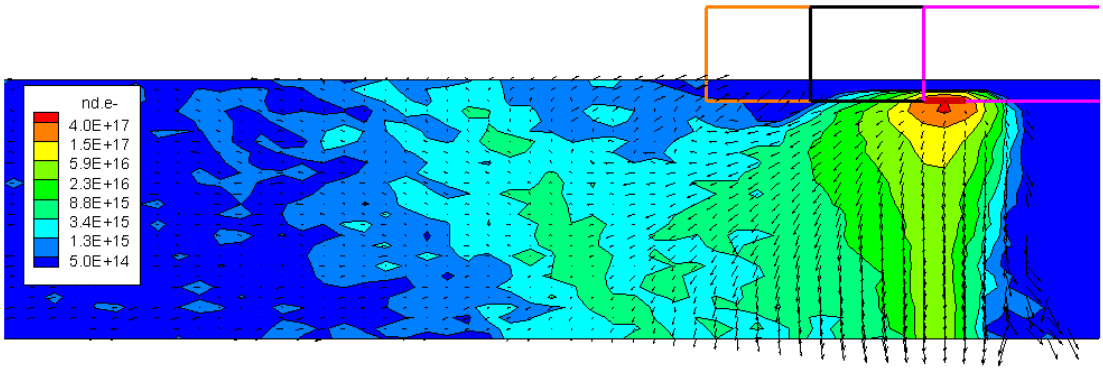

(c) Electron Density

Figure 8. Preliminary results showing plasma potential, ion density, and electron density for the case of no magnetic field.

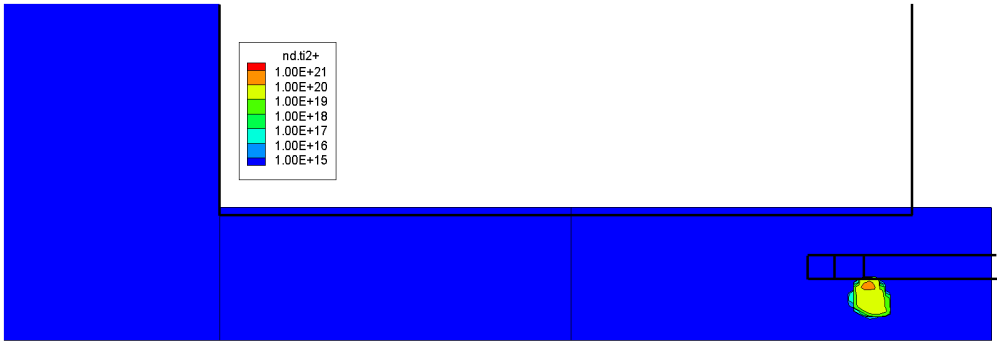

(a) 10,000

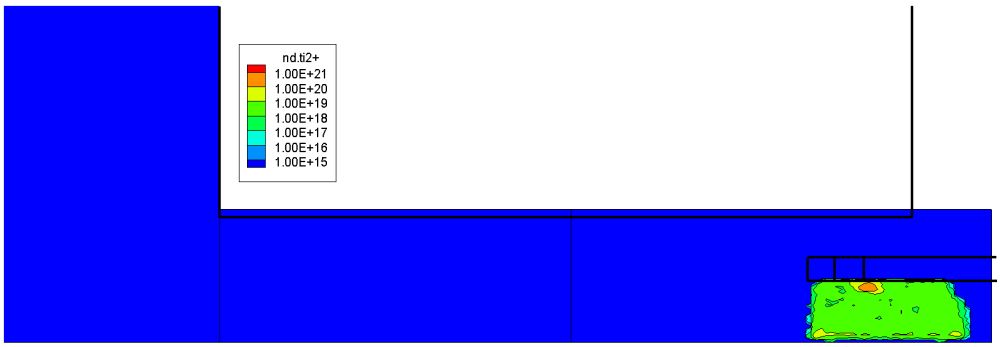

(b) 25,000

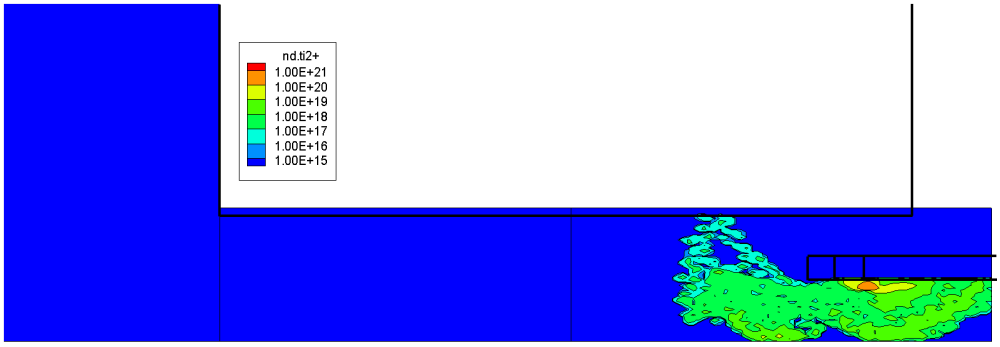

(c) 50,000

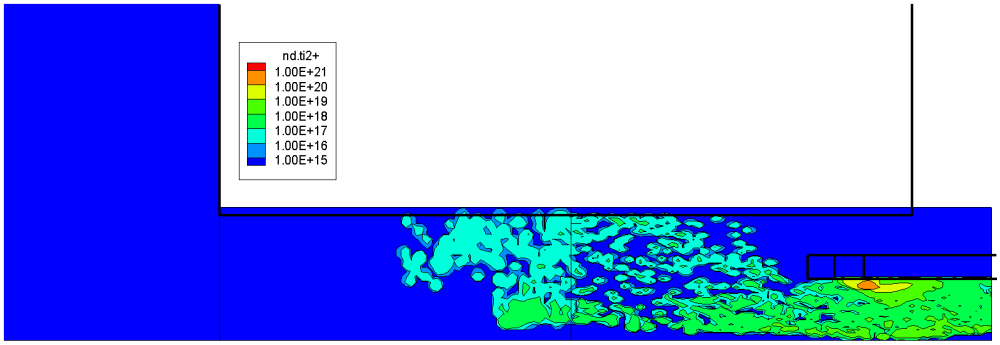

(d) 100,000

Figure 9. Preliminary results of ion density on the full domain.

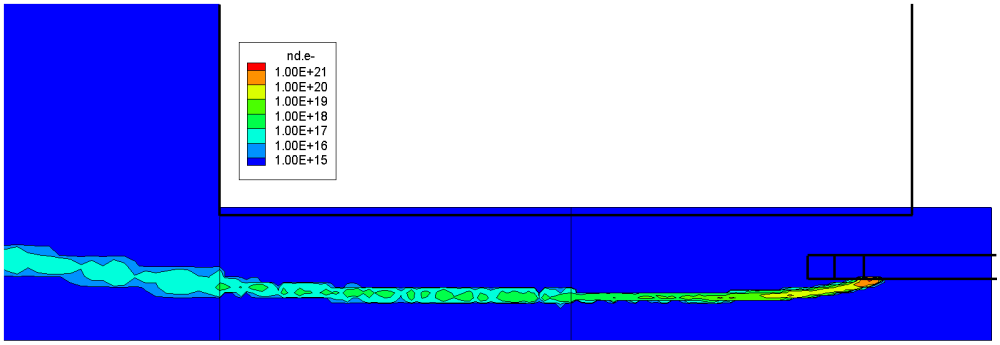

(a) 10,000

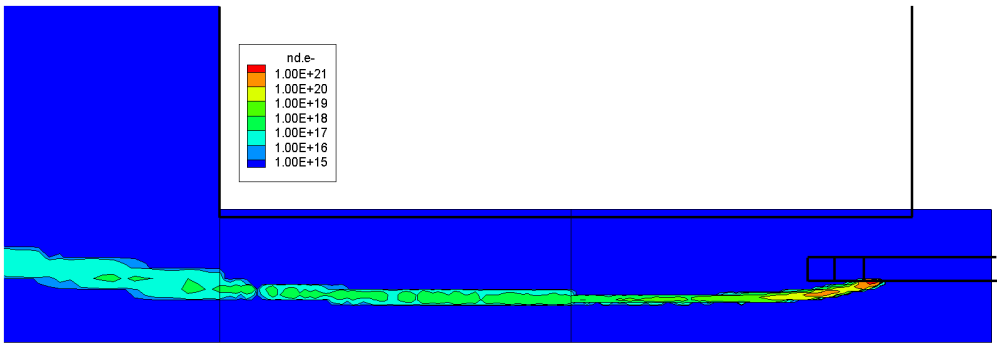

(b) 25,000

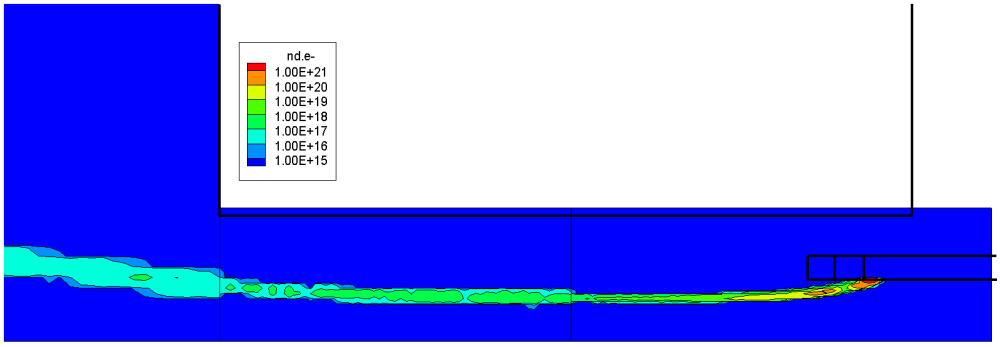

(c) 50,000

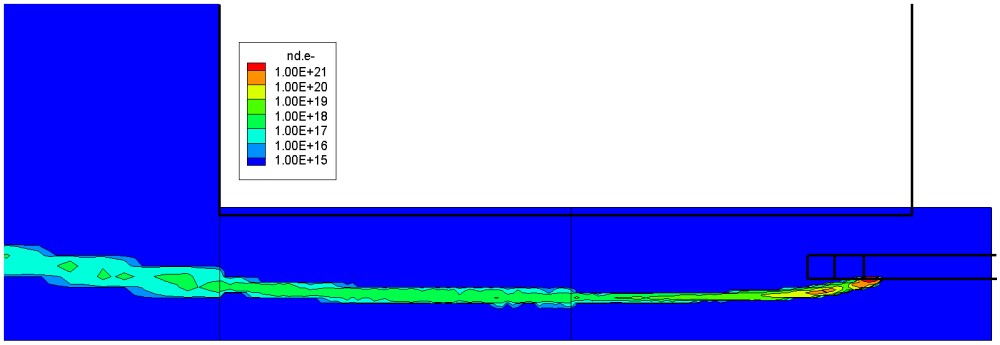

(d) 100,000

Figure 10. Preliminary results of electron density on the full domain.

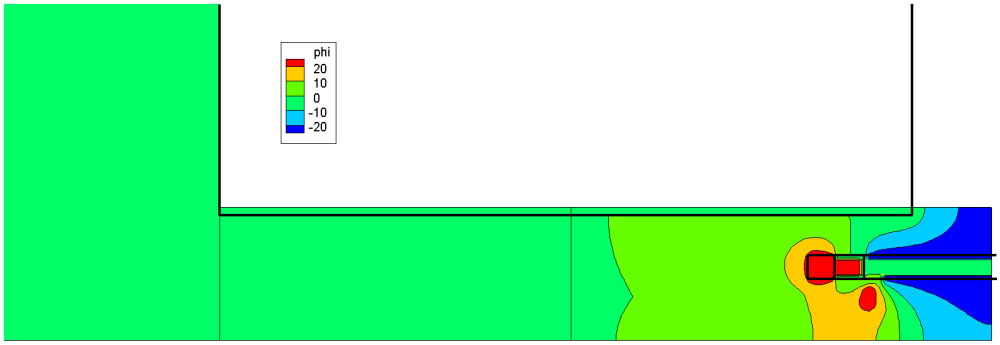

(a) 10,000

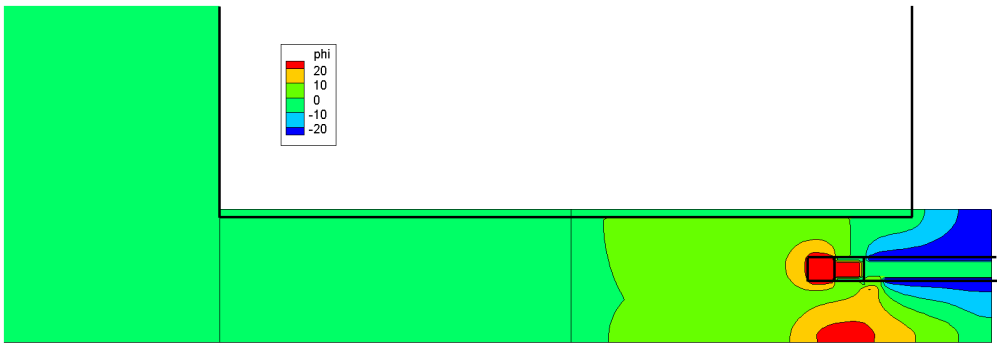

(b) 25,000

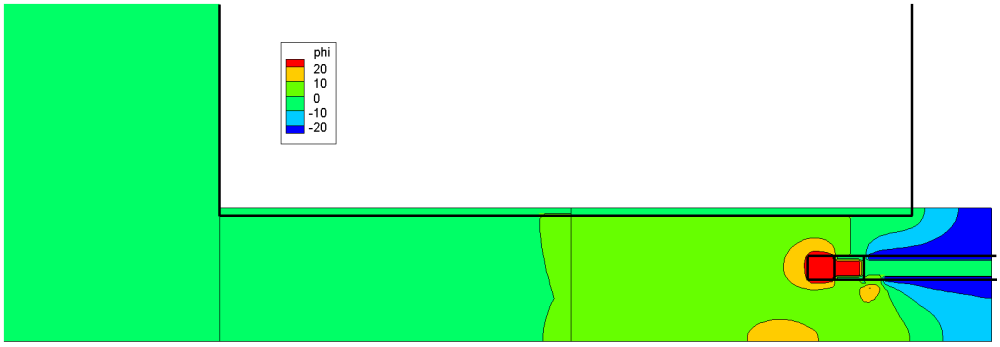

(c) 50,000

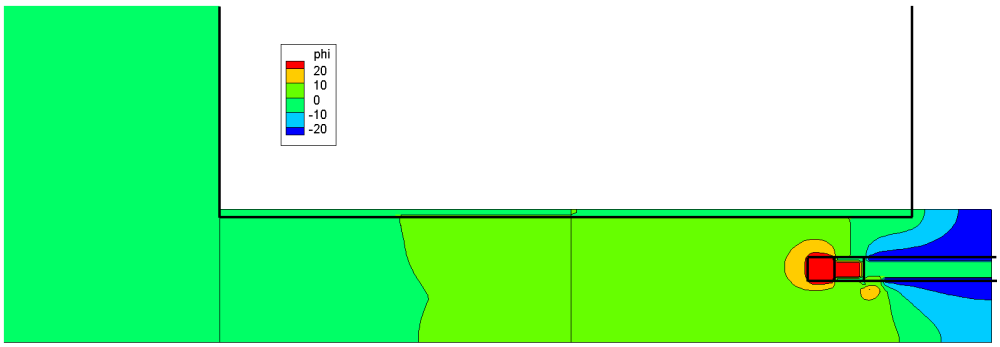

(d) 100,000

Figure 11. Preliminary results of plasma potential on the full domain.

[8]Brieda, L. and Keidar, M., "Development of the Starfish Plasma Simulation Code and Update on Multiscale Modeling of Hall Thrusters," *48th AIAA Joint Propulsion Conference*, Atlanta, GA, 2012.

[9]Brieda, L., Zhuang, T., and Keidar, M., "Towards Near Plume Modeling of a Micro Cathode Arc Thruster," *49th AIAA Joint Propulsion Conference*, San Jose, CA, 2013.

[10]Anders, A. and Yushkov, G. Y., "Ion flux from vacuum arc cathode spots in the absence and presence of a magnetic field," *Journal of Applied Physics*, Vol. 91, No. 8, 2002.

[11]Juttner, B., "Properties of arc cathode spots," *Le Journal de Physique IV*, Vol. 7, No. C4, 1997.